THE ASTROPHYSICAL JOURNAL, 389:196–207, 1992 April 10

NEAR-INFRARED SPECTRA AND CLASSIFICATION DIAGNOSTICS OF SEYFERT GALAXIES[1]

DONALD E. OSTERBROCK, HIEN D. TRAN, AND SYLVAIN VEILLEUX[2]
University of California Observatories/Lick Observatory, and Board of Studies in Astronomy and Astrophysics, University of California, Santa Cruz, CA 95064
Received 1991 July 9; accepted 1991 October 8

ABSTRACT

In this second paper of the series, observational results of our spectroscopic survey of Seyfert galaxies in the near-infrared are presented, and the potential for using emission-line ratios in this spectral region as a classification diagnostic tool is examined. Near-infrared CCD spectra, which cover the range $\lambda\lambda$7000–10000 at nominal resolution FWHM $\approx$ 12 Å, of 15 additional Seyferts and two starburst galaxies were obtained with the Lick Observatory 3 m Shane telescope. Relative emission-line intensities from these observations, in combination with measurements from our first paper (Osterbrock, Shaw, & Veilleux) and those of Morris & Ward as well as additional Lick observations and measurements of new, high signal-to-noise ratio optical spectra of many of these objects, are used to study the diagnostic diagrams involving [S III] $\lambda\lambda$9069, 9531/Hα, [O II] $\lambda\lambda$7320, 7330/Hα, [S II] $\lambda\lambda$6716, 6731/Hα, and [O III] λ5007/Hβ. Comparisons are made in these diagrams between observational data from the active galaxies and published measurements of H II region–like objects, as well as with predictions from simple one-component models calculated for the two types of objects. Our results suggest that diagnostic diagrams using near-IR lines such as [O II] $\lambda\lambda$7320, 7330 and [S III] $\lambda\lambda$9069, 9531 promise to provide a powerful method in classifying emission-line galaxies. Most but not all the diagnostic diagrams can be understood on the basis of photoionization models. There may be some heating due to relativistic electrons in addition to photoionization in active galactic nuclei (AGNs), but this is not at all clear.

Subject headings: galaxies: nuclei — galaxies: Seyfert — infrared: galaxies

1. INTRODUCTION

Extensive spectroscopic work on Seyfert galaxies has been chiefly confined to the optical region (~3500–7500 Å). With the advent of CCD detectors, reliable study of the emission-line spectra of these objects can be extended to the near-infrared region to beyond 10000 Å. The main use of the near-IR relative line intensities is to test and improve our understanding of the ionization and heating mechanisms in AGNs. By extending the spectral range observed, we hope to increase the number of emission lines and ions available for investigation. A large number of active galaxies, mostly in the southern hemisphere, have been studied spectrophotometrically in the near-infrared region by Morris & Ward (1988). More recently, our group at Lick Observatory has begun surveying Seyfert galaxies in the near-IR region also, and the first results were presented by Osterbrock, Shaw, & Veilleux (1990, hereafter Paper I). It confirmed that the strongest emission lines in the near-IR spectral region are [S III] $\lambda\lambda$9069, 9531, which are strong and almost ubiquitous in Seyfert galaxies and ionized nebulae, like [O III] $\lambda\lambda$4959, 5007 in the previous row of the periodic table. Together with [S III] λ6312, they provide a mean temperature measurement in the S^{++} emission zone.

A few additional lines due to other ions are also found in this spectral region among the Seyfert galaxies surveyed, the next strongest being He I λ10830. The CCD sensitivity is dropping rapidly at this wavelength, and most of our Seyfert spectra do not include it. Other lines observed include, in approximate order of strength and frequency of occurrence, [O II] $\lambda\lambda$7320, 7330, [Ar III] $\lambda\lambda$7136, 7751, and [Ni II] λ7378. Still weaker and not present in all Seyferts are [Ar V] λ7006, He I λ7065, [Fe II] λ7155, [Fe XI] λ7892, O I λ8446, and [Fe II] λ8617. Also seen in a number of these objects is an as yet unidentified "λ9212" feature (Morris & Ward 1988). Another application of measurements of lines in this region is the use of the relative strengths of [S III] $\lambda\lambda$9069, 9531 and [S II] $\lambda\lambda$6716, 6731 as a method of distinguishing between photoionization and shock heating mechanisms in active galaxies, to resolve the question of the nature of the ionization mechanisms in LINERs (Diaz, Pagel, & Terlevich 1985a; Diaz, Pagel, & Wilson 1985b; Kirhakos & Phillips 1989, hereafter KP89).

Since the publication of Paper I, we have obtained spectra of 15 additional Seyfert and two starburst galaxies in the near-IR. In this paper, we present the results for these objects. Furthermore, we present additional information on the classification of AGNs, extending the optical diagnostic tools of e.g., Baldwin, Phillips, & Terlevich (1981) and Veilleux & Osterbrock (1987, hereafter VO87). In § 2 the observations are described, along with additional measurements compiled from the literature. Diagnostic diagrams based on all these data are presented in § 3. In § 4, these diagrams are discussed and compared with their optical counterparts and with theoretical models. Our general conclusions are summarized in § 5.

2. OBSERVATIONS

All spectra presented in this paper were obtained at Lick Observatory with the Shane 3 m telescope, using the Cassegrain spectrograph with a TI 800 × 800 CCD detector. For the near-IR spectra, the observations were made using a slit width of 1".2 with a 300 lines mm^{-1} grating, giving a resolution (FWHM) of ~12 Å and covering a spectral range of ~6950–10100 Å. Since it is desirable to link up the near-IR spectral region with the optical region taken at about the same epoch, we also obtained optical spectra whenever possible with the same spectrograph but using a different 300 lines mm^{-1}

[1] Lick Observatory Bulletin, No. 1202.
[2] Present address: Institute for Astronomy, University of Hawaii, 2680 Woodlawn Drive, Honolulu, HI 96822.

TABLE 1

LOG OF OBSERVATIONS FOR THE RED AND NEAR-INFRARED SPECTRAL REGIONS

Object	Type	UT Date	λ_c	Exposure (minutes)
Mrk 530 = NGC 7603	Seyfert 1	1988 Oct 8	8520	90
		1988 Nov 5	6320	35
I Zw 1	Seyfert 1	1988 Oct 7	8520	90
		1988 Nov 5	6320	40
II Zw 136	Seyfert 1	1988 Oct 7	8520	90
		1988 Nov 5	6320	20
III Zw 77	Seyfert 1	1989 Apr 11	8800	75
		1989 May 12	8825	90
		1989 May 12	6330	30
NGC 3227	Seyfert 1.5	1989 Jan 31	6300	20
NGC 5548	Seyfert 1.5	1989 Jan 29	8517	60
		1989 Jan 31	6300	5
		1989 Jan 31	6300	5
Mrk 6	Seyfert 1.5	1988 Oct 7	8520	60
Mrk 359	Seyfert 1.5	1988 Oct 8	8520	90
		1988 Nov 5	6320	40
Mrk 704	Seyfert 1.5	1989 Apr 11	8800	90
		1989 Apr 12	6330	30
Mrk 975	Seyfert 1.5	1988 Oct 7	8520	90
NGC 1068	Seyfert 2	1988 Oct 8	8520	45
		1988 Oct 8	8520	15
NGC 4388	Seyfert 2	1989 May 11	8645	57
		1989 May 12	8825	60
		1989 May 12	6320	15
Mrk 917 = MCG 05-53-09	Seyfert 2	1988 Oct 7	8520	90
		1988 Nov 5	6320	25
Mrk 1157 = NGC 591	Seyfert 2	1988 Oct 8	8520	90
Mrk 1388	Seyfert 2	1989 Apr 12	8705	60
		1989 Apr 12	8705	60
		1989 Apr 12	6330	35
I Zw 92 = Mrk 477	Seyfert 2	1989 May 11	8645	70
		1989 May 12	8825	75
		1989 May 12	6320	15
NGC 23 = Mrk 545	Starburst	1988 Oct 7	8520	60
NGC 7714 = Mrk 538	Starburst	1988 Oct 8	8520	60

grating, covering the red spectral region $\lambda\lambda$4750–7900. Table 1 gives a journal of the observations for both the near-IR and red spectral regions. Here λ_c is the approximate central wavelength of the exposure.

For a number of objects, our previous optical spectra in the red either were at too short a wavelength to overlap with the near-infrared spectra, or the signal-to-noise ratio quality at the red end was too low to allow a reliable connection to the near-IR spectra. For these objects, we also obtained spectra in the deep red region with sufficient total exposure time to ensure a good signal-to-noise ratio, while not saturating the Hα + [N II] complex. The journal of these observations (which cover the spectral region $\lambda\lambda$5350–8550) is presented in Table 2.

2.1. *Reduction and Analysis*

The basic data reduction for the near-IR spectra has been described in Paper I. We used this same procedure for reducing the deep red spectra listed in Table 2. For the red spectra, the basic data reduction (i.e., spectrum extraction from the raw images, wavelength calibration) is identical to that used for the near-IR spectra, except that known sky lines are used to correct the zero point of the wavelength scale (see De Robertis & Osterbrock 1986). The removal of atmospheric absorption bands and flux calibration procedures are slightly simpler than those used for the near-IR spectra. The principal atmospheric bands in the optical region are the O_2 bands $\lambda\lambda$6870, 7620 (B and A bands). They were removed simply by dividing the object spectra by a smoothed and spline-fitted (but retaining both atmospheric bands) flux curve derived from a standard star spectrum, obtained at similar zenith distance to the object's. This is the main difference between the fluxing procedures used for the optical and near-IR spectra. Simple division by the star flux curve would not suffice for the latter because of the highly variable strengths of the H_2O bands present throughout much of the near-IR spectral range covered. Instead, as detailed in Paper I, careful determination of the amount of absorption correction separately for each band is required. Examples of the final reduced spectra of Mrk 6, a Seyfert 1.5 galaxy, Mrk 1157, a Seyfert 2 galaxy, and NGC 7714, a starburst galaxy, are shown in Figures 1, 2, and 3 respectively.

The fluxes of the single emission lines were measured with standard Lick Observatory routines as described in Paper I and Osterbrock & Shaw (1988). For blended lines such as the Hα + [N II] complex, the program GAUSS (Dahari 1985) was used. It fits as many as four Gaussian profiles to the blended feature assuming the intensity ratio [N II] λ6583/λ6548 = 2.90 and the known fixed wavelength separations between the [N II] lines and Hα. The broad (b) and narrow (n) components of Hα and Hβ of the Seyfert 1.5 galaxies in our sample were also separated using GAUSS. This was done by an iterative procedure, adjusting the strengths and widths of both the broad and narrow Gaussian profiles, as well as their relative positions, until the synthetically calculated blended profile satisfactorily matched the observed profile. Typically, the mean root-mean-square residuals from such deblending is $\sim$1%. Based on previous experience with similar spectral data, the

TABLE 2

LOG OF OBSERVATIONS FOR THE DEEP RED SPECTRAL REGION ($\lambda\lambda$5350, 8550)

Object	Type	UT Date	Exposure (minures)
NGC 7469	Seyfert 1.5	1990 Nov 13	20
		1990 Nov 13	10
		1990 Nov 13	10
Mrk 6	Seyfert 1.5	1990 Nov 12	25
		1990 Nov 12	20
Mrk 704	Seyfert 1.5	1990 Nov 12	20
		1990 Nov 12	25
		1990 Nov 12	25
Mrk 975	Seyfert 1.5	1990 Nov 12	30
		1990 Nov 12	30
		1990 Nov 13	20
		1990 Nov 13	40
		1990 Nov 13	40
Mrk 1	Seyfert 2	1990 Nov 13	30
Mrk 3	Seyfert 2	1990 Nov 12	25
		1990 Nov 12	20
Mrk 917	Seyfert 2	1990 Nov 12	20
		1990 Nov 12	20
		1990 Nov 12	20
		1990 Nov 13	20
		1990 Nov 13	40
Mrk 1157	Seyfert 2	1990 Nov 12	30
		1990 Nov 12	30
NGC 23	Starburst	1990 Nov 12	10
		1990 Nov 12	50
		1990 Nov 13	20
		1990 Nov 13	60
NGC 7714	Starburst	1990 Nov 12	45
		1990 Nov 12	10
		1990 Nov 13	5
		1990 Nov 13	5

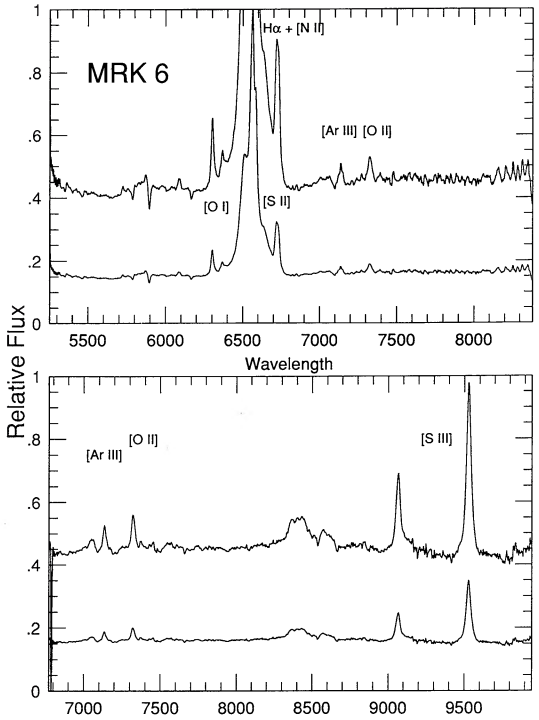

FIG. 1.—Deep red (*upper panel*) and near-infrared (*lower panel*) spectra of Mrk 6, a Seyfert 1.5 galaxy, in the rest system of the object, plotted at two scales to show stronger and weaker lines.

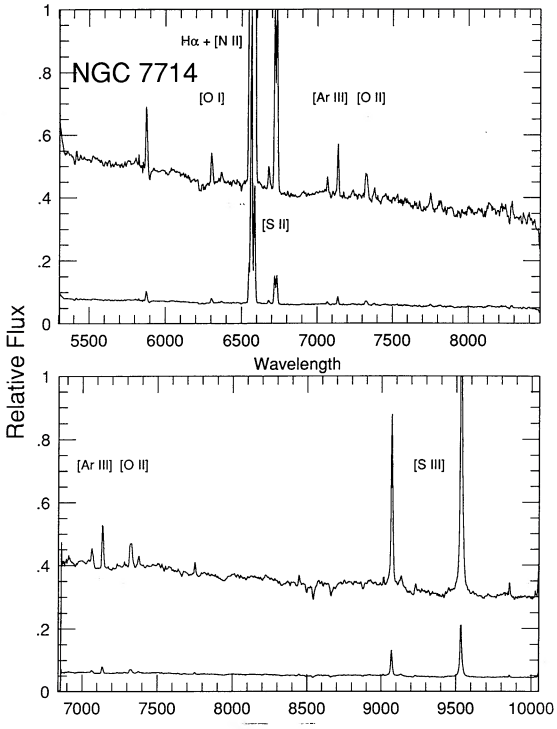

FIG. 3.—Deep red (*upper panel*) and near-infrared (*lower panel*) spectra of NGC 7714, a starburst galaxy, in the rest system of the object, plotted at two scales to show stronger and weaker lines.

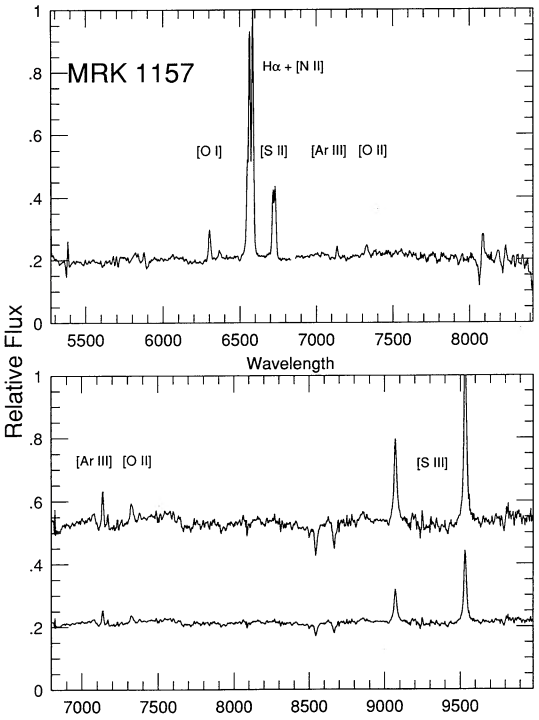

FIG. 2.—Deep red (*upper panel*) and near-infrared (*lower panel*) spectra of Mrk 1157, a Seyfert 2 galaxy, in the rest system of the object. Lower panel is plotted at two scales to show stronger and weaker lines.

relative flux measurements on strong, well-defined lines in the optical region have uncertainties of $\lesssim 10\%$. For the weaker lines (e.g., [N II] $\lambda 7378$), the uncertainties are somewhat larger and the measured fluxes are only accurate to within 10%–30%. An indication of the uncertainties can also be obtained from a comparison between our measurements in this paper or in Paper I and those of KP89 for the three Seyfert galaxies measured independently by them (NGC 1068, Mrk 3, and Mrk 6). We find that the ratios between our measurements and those of KP89 to have the mean values [S III]/Hα = 1.02 $\pm$ 0.26, and [S II]/Hα = 0.88 $\pm$ 0.19 (standard deviations).

To link up the intensity scales in the optical and near-IR regions, we used the strongest lines that could be identified and measured in both regions. They should be lines that are least affected by absorption in the atmospheric A band or the $\lambda 7250$ H_2O band. The lines usually used for this connection were [O II] $\lambda 7325$ and/or [Ar III] $\lambda 7136$, and in a few objects [Ni II] $\lambda 7378$ and [Fe XI] $\lambda 7892$, if they were strong enough to be measured accurately. Table 3 gives the observed relative line fluxes in the near-IR region for each object, together with our optical line flux measurements either from the recent red optical scans listed in Table 1 or from the deep red scans listed in Table 2, or both. Only the stronger lines which can be measured with fairly good accuracy are included. Given in the table are the ions responsible for the emission, the approximate wavelength of the line or blend, and the observed ratio of fluxes with respect to the narrow component of Hα. Note that [S II] $\lambda 6724 = (\lambda 6716 + \lambda 6731)$ and [O II] $\lambda 7325 = (\lambda 7320 + \lambda 7330)$. In this and later tables, those values uncertain by about a factor of 2 or more are noted with a colon (:). For Seyfert 1.5 galaxies, we also list in the table the relative flux of the broad components of Hα, obtained by using the deblending technique described above. It should be noted that

TABLE 3

OBSERVED RED AND NEAR-IR LINE FLUX RATIONS

Name	[N II] 6548	Hα(broad) 6563	[N II] 6583	[S II] 6724	[Ar III] 7136	[O II] 7325	[Ni II] 7378	[Fe XI] 7892	[S III] 9069	[S III] 9531
NGC 23	18.9	...	65.3	37.3	1.67:	...	1.93:	...	15.4	25.8
NGC 1068[a]	58.8	...	173.	32.9	11.4	8.08	1.36	...	36.2	90.1
NGC 3227	60.4	269.	175.	45.6	...	5.46	2.03	...	...	...
NGC 4388	27.5	...	79.8	80.7	11.5	8.80	...	...	38.6	103.4
NGC 5548	24.8	1000.	71.8	16.1	7.09	5.00	1.42	...	11.9	23.5
NGC 7714	9.02	...	39.1	18.2	2.42	2.38	0.855	...	11.0	29.4
Mrk 6	20.0	435.[b]	57.6	32.0	4.99	7.13	0.941	...	28.4	61.6
Mrk 359	52.2	447.[c]	152.	40.7	8.19:	13.0	...	...	35.7	64.2
Mrk 704	9.83	1340.	28.5	14.7	5.06	4.95	...	13.1	13.8	34.7
Mrk 917	28.4	...	82.4	35.0	3.44	8.53	2.72:	...	16.4	51.5
Mrk 975	21.3	920.	61.6	14.4	4.10	7.22	...	...	8.93	29.8
Mrk 1157	43.6	...	117.	62.2	8.2:	7.2	2.40	...	34.5	85.8
Mrk 1388	14.8	...	43.0	16.4	8.39	13.2	...	...	27.6	60.4
I Zw 92	14.7	...	42.7	36.4	8.67	13.0	1.96:	...	18.0	52.0

NOTE.—Hα(narrow) = 100.

[a] Using Hα/(Hα + [N II]) = 0.296 from Koski 1978.

[b] From Koski 1978.

[c] From Veilleux 1991.

the ratios Hα(b)/Hα(n) given are somewhat uncertain not only because of the deblending process, but also because of the variability of the broad line regions. We tried to minimize any such variability effect by obtaining the optical and near-IR data at the same epoch whenever possible. Since we have no new optical data for NGC 1068, we used the decomposition of the Hα + [N II] complex by Koski (1978). The adopted ratio [N II]/Hα = 2.38 agrees to within 1% with the more recent value that Cecil, Bland, & Tully (1990) measured for the total NLR by imaging spectrophotometry with a Fabry-Perot interferometer. We also adopted the Hα(n + b)/Hα(n) and [N II]/Hα ratios for Mrk 6 from Koski (1978).

Because of their strong broad Balmer-line components (which make it difficult to isolate the weak narrow components of these lines), all Seyfert 1 galaxies in the sample have been excluded from diagnostic classification, and their measurements are listed separately in Table 4. However, two "narrow-line Seyfert 1s" (Osterbrock & Pogge 1985) are present in the sample. These are Mrk 359 (from this study) and Mrk 1126 (from Paper I). Recently, Veilleux (1991) measured the narrow components of Hα and Hβ on high-resolution spectra of Mrk 359 giving ratios Hα(b)/Hα(n) = 4.47 (as noted in Table 3) and Hα(n)/Hβ(n) = 3.27. We used the first of these values to separate the narrow component of Hα and the second to determine the amount of reddening correction in Mrk 359. For Mrk 1126, classified as a narrow-line Seyfert 1.5 by Osterbrock & Pogge (1985), the narrow components of Hα and Hβ could be measured on our existing lower resolution spectra.

Table 4 lists the observed measurements of two of the four Seyfert 1 galaxies observed in this study. Again, we include only the stronger lines. Note that here the relative fluxes are given with respect to [S II] λ6724. No effort has been made to deblend [N II] from Hα in these galaxies because of the overwhelming strength of the broad components of Hα and the large uncertainties involved. Also, as mentioned in Paper I, since the emission-line spectrum of I Zw 1 is severely blended, being dominated by many Fe II emission lines, no attempt was made to measure its relative line intensities. For Mrk 530, the quality of our spectra is not sufficient to connect the intensity scales of the red and near-IR regions. Its measured ratio (Hα + [N II])/[S II] λ6724 = 21.9 and [S III] λ9531/λ9069 = 2.60.

The measured relative fluxes shown in Table 3 were then corrected for interstellar extinction and the resulting relative intensities are given in Table 5. Anticipating the selection of lines used for classification in § 3, we list only the corrected ratios for [S II] λλ6724, [O II] λλ7325, and [S II] λ9069 + λ9531, given with respect to Hα(n), and [O III] λ5007, given with respect to Hβ(n). The necessary reddening correction was found from the Balmer decrement, assuming an intrinsic ratio Hα/Hβ = 3.1 for AGNs. As discussed in VO87, this value is larger than the pure recombination value 2.86 at $T = 10^4$ K and $N_e = 10^4$ cm^{-3} (Hummer & Storey 1987) commonly used to correct line ratios for reddening in H II regions, due to the large partially ionized zone in AGNs and the importance of collisional excitation there. The value 3.1 is in better agreement with photoionization models (Ferland & Netzer 1983; Pequignot 1984) and observational results (Gaskell 1984; Gaskell & Ferland 1984; Malkan 1983; Halpern & Steiner 1983). Although an even higher intrinsic value, 3.4, has been suggested (Binette et al. 1990) for Seyfert 2 galaxies, we adopt 3.1 in the present study for consistency with VO87. For

TABLE 4

OBSERVED RED AND NEAR-IR LINE RATIOS FOR SEYFERT 1 GALAXIES

Object	Hα + [N II]	[S II] 6724	[Ar III] 7136	[O II] 7325	[Ni II] 7378	[Fe XI] 7892	[S III] 9069	[S III] 9531
II Zw 136	73.4	1.00	...	...	...	...	0.768	...
III Zw 77	68.6	1.00	0.451	0.634	...	0.809	2.73	5.64

the Seyfert 1.5 galaxies, only the narrow components of Hα and Hβ were used in the line ratios and to determine the reddening correction. For lack of detailed knowledge of the properties of dust in external galaxies, the average interstellar extinction curve determined from relatively nearby stars in our own Galaxy, as listed in Table 7-2 of Osterbrock (1989), was used to correct the relative fluxes of Table 3 for reddening. The reddening constant $c = E(B-V)/0.77$ for each object is listed in Table 5 together with the corrected line intensity ratios. The first entry in the last column gives references to the Hα(n)/Hβ(n) ratios from which the reddening correction was derived. For many of the objects, they are from our new measurements; for the remainder we have adopted the narrow-line Balmer ratios from the literature. The second entry gives references to the deblending of Hα and [N II], and of the narrow from the broad components of Hα and Hβ for the Seyfert 1.5 galaxies. The third entry gives references to the [O III] λ5007/Hβ intensity ratios. Preference is given to data taken in a more or less homogeneous way by our group at Lick.

2.2. *Additional Near-IR Data Sample from the Literature*

The main use of the near-IR relative line intensities is to test and extend our understanding of AGNs with regard to ionization, temperature and density diagnostics, ion abundances, and spectral classification. These are the subjects to which the present paper is addressed. One advantage of using lines in the near-IR is that they are significantly less sensitive to dust extinction because of the longer wavelengths. As an example, the usefulness of the [S III] λλ9069, 9531 lines as a tool for examining the ionization mechanisms in LINERs has been demonstrated by Diaz et al. (1985a) and KP89. On the basis of our larger sample of AGNs, in this paper we examine the classification diagnostics, using near-infrared emission lines, and thus extend the optical classification tools of VO87. In choosing the lines to be used for such a near-IR classification scheme, we should consider all the criteria listed in VO87. The lines must be present in the spectra of most AGNs and emission-line galaxies. A line need not be exceptionally strong (like Hα or [O III] λ5007); rather, it need only be easily detectable, with a flux measurable with fairly good accuracy in most emission line galaxies. There are not a great number of strong lines in the near-IR region. Two exceptions are [S III] λλ9069, 9531 which, however, are ~2700 Å from Hα, the nearest Balmer line, and therefore are sensitive to reddening-correction and flux calibration errors. The high-*n* Paschen lines near the [S III] pair are too weak to be accurately measured in most Seyfert galaxies. Another quite easily detectable line is the [O II] λ7325 blend, which is present in most AGN and H II regions spectra. The [Ar III] λ7136 line is similar in strength to [O II] λ7325, but presently the amount of available data for it in H II regions is considerably less than that for the [O II] lines. By virtue of their strengths and ubiquity, therefore, we have chosen [S III] λλ9069, 9531 and [O II] λ7325 in the near-IR, to use along with [S II] λλ6716, 6731 and [O III] λ5007 in the optical region for these additional spectral diagnostics.

Unlike the optical data available to VO87, there are relatively fewer measurements of the [S III] lines to date. In order to add as many data as possible, we have collected near-IR data for AGNs from Morris & Ward (1988), as listed in Table 6. Our AGN sample includes not only narrow-line Seyfert 2 galaxies (as in VO87) but also the narrow-line spectra of the Seyfert 1.5s, using only the narrow components of H I in the line ratios. Since the measurements of Morris & Ward (1988) are all given with Hα + [N II] blended and/or broad and narrow lines of Balmer lines unseparated, we either used published deblended optical data, or deblended and measured them ourselves from the large collection of optical data at Lick Observatory. References for the optical data and [N II]/Hα, Hα(n + b)/Hα(n), and Hβ(n + b)/Hβ(n) ratios are noted in the last column in Table 6 in a similar manner to that of Table 5. Also listed are the near-IR data for LINERs from KP89, along with the optical data taken from references given in it. We have also included in the table all those objects from Paper I whose near-IR data could be linked up with the optical measurements. Quite recently, Perez et al. (1990) have identified two sources from the *IRAS* Point Source Catalog, IRAS 01475−0740 and IRAS 20210+1121, as Seyfert 2 galaxies. This identification was based on the presence of high ionization lines, on their emission line widths, and relative intensity ratios, which include those of the near-IR [O II] and [S III] lines. We have added two new sources in our AGN sample in

TABLE 5

REDDENING-CORRECTED LINE INTENSITY RATIOS

Object	Type	c	Hα(n) / Hα(b + n) + [N II]	[S II] 6724	[S III] 9069+9531	[O III][a] 5007	[O II] 7325	References[b]
NGC 23	Starburst	0.27	0.54	0.369	0.337	0.466	...	2, 1, 1–2
NGC 1068	Seyfert 2	0.43	0.30	0.330	0.921	12.68	0.074	4, 4, 4
NGC 4388	Seyfert 2	0.34	0.48	0.794	1.100	10.78	0.083	1, 1, 1
NGC 5548	Seyfert 1.5	0.13	0.084	0.165	0.331	9.88	0.047	5, 1, 1 & 5
NGC 7714	Starburst	0.85	0.68	0.175	0.214	1.67	0.020	1, 1, 1
Mrk 6	Seyfert 1.5	0.50	0.16	0.313	0.619	9.77	0.064	4–5, 4–5, 1 & 4–5
Mrk 359	NL Seyfert 1	0.063	0.12	0.406	0.953	9.04	0.128	6, 6, 1 & 6
Mrk 704	Seyfert 1.5	0.059	0.059	0.147	0.464	6.57	0.049	5, 1 & 5, 1 & 5
Mrk 917	Seyfert 2	1.32	0.47	0.330	0.253	5.74	0.064	1, 1, 1
Mrk 975	Seyfert 1.5	0.34	0.11	0.142	0.301	7.02	0.067	5, 1 & 5, 1 & 5
Mrk 1157	Seyfert 2	0.52	0.38	0.607	0.815	9.72	0.064	2, 1, 1–2
Mrk 1388	Seyfert 2	0.39	0.63	0.155	0.656	9.91	0.117	1 & 3, 1, 1 & 3
I Zw 92	Seyfert 2	0.14	0.63	0.362	0.631	9.12	0.126	1, 1, 1

NOTE.—Hα(narrow) = 1.00.

[a] Intensity ratio is relative to Hβ(narrow) = 1.00.

[b] Reference key: (1) This paper; (2) Veilleux & Osterbrock 1987; (3) Osterbrock 1985; (4) Koski 1978; (5) Cohen 1983; (6) Veilleux 1991. See text, § 2.1, for explanation of entries.

TABLE 6

REDDENING-CORRECTED LINE INTENSITY RATIOS FOR AGNs

Object	Type	c	$\frac{H\beta(b)}{H\beta(n)}$	$\frac{H\alpha(b)}{H\alpha(n)}$	$\frac{H\alpha(n)}{H\alpha(b+n)+[N\ II]}$	[S II] 6724	[S III] 9069+9531	[O III][a] 5007	[O II] 7325	Reference[b]
Morris & Ward 1988										
NGC 5506	Seyfert 2	1.08	0.	0.	...	0.698	0.561	6.99	0.072	9, 10, 10 & 4
NGC 5643	Seyfert 2	0.86	0.	0.	...	0.718	0.630	13.65	0.060	9, 11, 11 & 4
NGC 6221	?	0.78	0.	0.	0.531	0.260	0.362	0.568	0.018	1, 3, 4
NGC 6814	Seyfert 1.5	0.95	42.6	16.6	0.047	0.950	1.226	30.6	...	1, 1, 4
Mrk 509	Seyfert 1.5	0.42	14.3	12.1	0.079	0.147	0.238	5.03	...	1, 1, 4
Mrk 841	Seyfert 1.5	0.33	20.8	18.9	0.049	0.260	0.414	12.11	...	1, 2, 4
Mrk 871	Seyfert 1.5	0.088	11.4	17.0	0.054	0.243	0.730[c]	8.90	...	1, 1, 4
Mrk 926	Seyfert 1.5	0.0	7.5	23.8	0.039	0.902	0.534	8.20	0.194	2–3, 2, 4
Kirhakos & Phillips 1989										
NGC 1052	LINER	0.0	0.	0.	...	1.109	0.610	2.23	0.193	12, 14, 12
NGC 1097	LINER	0.76	0.	0.	...	0.889	0.859	2.91	...	9, 13, 13
NGC 1275	LINER	0.75	0.	0.	...	0.302	0.245	3.45	0.085	9, 15–16, 15–16
NGC 1433	LINER	0.4	0.	0.	...	1.01	0.340[d]	3.01	...	17, 17, 17
NGC 6240	LINER	1.6	0.	0.	...	0.95	0.185	1.26	0.09	20, 19, 4
NGC 7590	LINER	0.31	0.	0.	...	0.865	0.470	3.62	...	17, 17, 17
PKS 1718−649	LINER	0.38	0.	0.	...	0.479	0.236	1.89	0.171	12, 18, 18
Paper I										
NGC 3227	Seyfert 1.5	0.48	...	2.7	0.165	0.446	0.945	10.87	0.059	2, 1, 1–2
NGC 4151	Seyfert 1.5	0.19	6.34	6.34	0.123	0.561	0.619	13.38	0.092	5, 5, 5
NGC 7469	Seyfert 1.5	0.67	...	2.92	0.210	0.209	0.381	4.15	0.026	2, 1, 1–2
Mrk 1	Seyfert 2	0.56	0.	0.	0.471	0.420	0.604	11.12	0.160	6, 6, 1 & 6
Mrk 3	Seyfert 2	0.63	0.	0.	0.424	0.529	0.571	12.65	0.098	6, 6, 1 & 6
Mrk 915	Seyfert 1.5	0.62	1.8	2.91	0.210	0.333	0.488	10.98	0.040	7, 1 & 7, 7
Mrk 1126	NL Seyfert 1	0.99	2.63	2.34	0.208	0.493	0.476	14.17	...	8, 1, 8
Perez et al. 1990										
IRAS 0147−074	Seyfert 2	1.56	0.	0.	0.556	0.320	0.312	6.31	0.034	21, 21, 21
IRAS 2021+112	Seyfert 2	0.96	0.	0.	0.522	0.130	0.244[e]	5.85	0.049	21, 21, 21

NOTE.—$H\alpha$(narrow) = 1.00.

[a] Intensity ratio is given relative to $H\beta$(narrow) = 1.00.

[b] Reference key: (1) This paper; (2) Cohen 1983; (3) Durret & Bergeron 1988; (4) Morris & Ward 1988; (5) Osterbrock & Koski 1976; (6) Koski 1978; (7) Osterbrock, Shaw, & Veilleux 1990; (8) Osterbrock & Pogge 1985; (9) Kirhakos & Phillips 1989; (10) Shuder 1980; (11) Phillips, Charles, & Baldwin 1983; (12) Fosbury et al. 1978; (13) Phillips et al. 1984; (14) Phillips et al. 1986; (15) Wampler 1971; (16) Shields & Oke 1975; (17) Diaz, Pagel, & Wilson 1985b; (18) Filippenko 1985; (19) Fried & Ulrich 1985; (20) Fosbury & Wall 1979; (21) Perez et al. 1990. See text, §§ 2.1 and 2.2, for explanation of entries.

[c] Only intensity for [S III] λ9531 was given in Morris & Ward 1988; we used the observed [S III] λ9531/[S III] λ9069 = 2.4 as given in Osterbrock, Shaw, & Veilleux 1990 to get total intensity for [S III].

[d] [S III] value denotes upper limit.

[e] Only intensity for [S III] λ9069 was given in Perez et al. 1990; used same ratio as above to derive the total intensity for [S III].

Table 6. All the published flux ratios from these papers, except those from KP89, were corrected for interstellar extinction using the same intrinsic $H\alpha/H\beta$ ratio and reddening curve described above.

For our near-IR spectral classification study, data for H II region–like objects were also needed. Our own sample of objects in the near-IR survey includes only two starburst galaxies, NGC 23 and NGC 7714. The rest of the near-IR data for H II regions were collected from the literature. A recent study of extragalactic H II regions by Garnett (1989) contains measurements of [O II] λ7325 and [S III] $\lambda\lambda$9069, 9531 for a large number of these objects. Near-infrared data for H II regions in the Magellanic Clouds and in our Galaxy are also available from Dennefeld & Stasinska (1983). Additionally, new data for the central part of NGC 1976, the Orion Nebula, are included from a recent paper by Osterbrock, Tran, & Veilleux (1992). Also, measurements for two emission-line nuclei, whose relative spectral line strengths most resemble those of H II regions, are included. They are NGC 1614 from KP89 and NGC 1672 from Diaz et al. (1985b). NGC 1672, however, is not a pure H II region galaxy and also has LINER spectral characteristics. Table 7 lists the relative emission line intensities corrected for reddening, for H II regions and H II region galaxies collected from the literature, using $H\alpha/H\beta = 2.86$ and the standard interstellar extinction curve. The sources of the optical data for these objects are cited in papers listed in the table. In a few cases where the combined [O III] (λ4959 + λ5007) emission-line fluxes were given, a calculated value of [O III] λ5007/[O III] λ4959 = 2.9 was used to separate the two.

3. RESULTS

Figures 4–7 give plots of the reddening-corrected line ratios for all the objects presented in this paper. In these diagrams, the narrow-line ratios for the AGNs (Seyfert 1.5 and Seyfert 2 galaxies) are plotted as filled symbols: circles if they were measured by us, squares if derived from Morris & Ward (1988), and pentagons denoting the two *IRAS* Seyfert 2 sources identified by Perez et al. (1990). The H II region objects are plotted as open squares, and the starburst galaxies as open circles. The LINERs are shown as filled triangles. The asterisk symbol

TABLE 7

REDDENING-CORRECTED LINE INTENSITY RATIOS FOR H II REGIONS

Object	[S II]/Hα 6724	[S III]/Hα 9069+9531	[O III]/Hβ 5007	[O II]/Hα 7325
		Garnett 1989		
NCC 604	0.110	0.238	2.08	0.01
NCC 595	0.110	0.365	1.43	0.015
IC 131	0.096	0.308	3.88	0.014
NCC 588	0.082	0.344	4.65	0.012
NCC 5471	0.071	0.169	6.76	0.013
IC 10	0.064	0.374	5.37	0.017
II Zw 40	0.053	0.161	7.86	0.011
NCC 4861	0.063	0.172	6.38	0.013
NCC 2363	0.031	0.113	7.08	0.0043
I Zw 123	0.082	0.127	...	0.017
Mrk 36	0.090	0.102	5.32	0.020
Mrk 600	0.066	0.097	6.60	0.011
I Zw 18	0.024	0.051	2.04	...
		Dennefeld & Stasinka 1983		
NGC 2467	0.066	0.249	1.91	0.03
Eta Car	0.091	0.396	2.24	0.01
M17	0.022	0.521	3.29	0.005
M16	0.078	0.251	1.42	...
M20	0.145	0.411	0.87	...
NGC 3576	0.047	0.974	3.32	0.026
N59A	0.045	0.282	5.34	...
N44B	0.065	0.371	7.94	...
N55A	0.039	0.348	2.71	...
N113D	0.074	0.410	2.36	...
N127A	0.065	0.399	2.30	0.012
N159A	0.034	0.332	4.60	...
N214C	0.160	0.335	2.88	...
N4A	0.044	0.327	4.15	...
N79E	0.109	0.257	1.28	...
N191A	0.128	0.353	0.75	...
N80	0.049	0.149	2.49	...
N83	0.106	0.178	3.14	...
N13	0.034	0.259	3.93	0.010
N32	0.129	0.114	0.22	0.0344
N81	0.042	0.254	5.25	0.017
N66	0.038	0.133	5.10	...
		Osterbrock, Tran, & Veilleux 1992		
NGC 1976	0.0237	0.704	3.02	0.0416
		Kirhakos & Phillips 1989		
NGC 1614	0.187	0.354	0.68	0.0146
		Diaz, Pagel, & Wilson 1985		
NGC 1672	0.300	0.240	0.968	...

denotes NGC 6221, an interesting case which will be discussed later. In Figure 4 it also denotes NGC 1672, an object intermediate between LINER and H II region galaxy. We do not have a measurement of [O II] λ7325 for it. Note that the sample presented in these diagrams (especially those involving [O II] λ7325, because of its relative weakness compared to [S III] λλ9069, 9531) is by no means a complete one. The objects were selected purely by the availability of the near-IR emission line data, especially [S III] λλ9069, 9531, and from these objects, only those with lines strong enough to be detected and measured are plotted. If some regions in the diagram are devoid of points, it does not necessarily mean that there are no objects which occupy these areas. Rather, it is possible that if we had a larger sample or sufficiently high-quality spectra for all the objects in the present sample to allow measurements of the

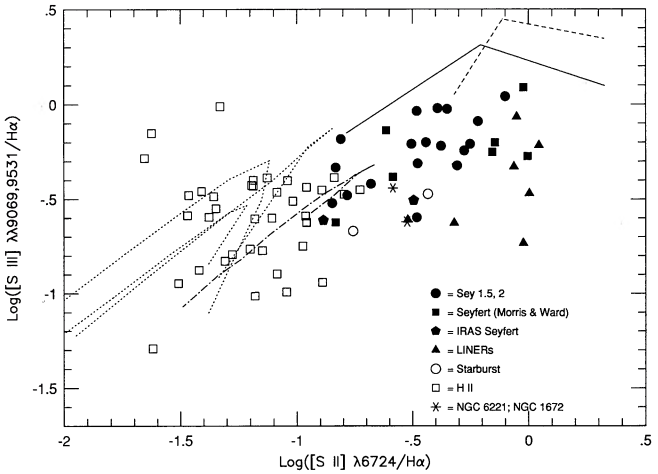

FIG. 4.—Reddening-corrected [S III] λλ9069, 9531/Hα vs. [S II] λ6724/Hα intensity ratios. Filled symbols denote Seyfert galaxies and LINERs; open symbols represent H II region–type objects. The solid curve represents AGN models of Stasinska (1984a) with $N_e = 10^3$ cm^{-3}, and the short dashed curve represents those with $N_e = 10^4$ cm^{-3}. In both curves, the ionization parameter Γ varies from 10^{-4} (*upper right*), through 10^{-3} to 10^{-2} (*lower left*). The dotted lines represent a sequence of models for extragalactic H II regions of Stasinska (1990) for $T_* = 32{,}500$, 40,000, and 55,000 K from top to bottom, respectively. The dash-dot line indicates H II region models of McCall, Rybski, & Shields (1985). The abundance ratio O/H ranges from 0.1 to 4.0 times the solar value, corresponding to T_* from 47,000 to 32,500 K along the curve.

weaker [O II] λ7325 lines, the apparent gaps might be filled in, forming, for instance, a continuous sequence between the AGNs and the H II regions.

One peculiar object marked by an asterisk in all the figures is NGC 6221. Its classification is somewhat uncertain. Phillips (1979) found that the partially resolved lines of Hα, [N II], and [S II] in a moderate-resolution (~5 Å) spectrum of its nucleus are narrower (FWHM $\lesssim$ 200 km s^{-1}) than normally found in Seyfert 2 galaxies, although Marshall et al. (1979) identified it as a possible X-ray source. In addition, its spectrum at lower resolution (25 Å) extending to the blue was noted for its absence of emission lines coming from a wide range of ionization. Considerably higher resolution data (1.5 Å) of Véron,

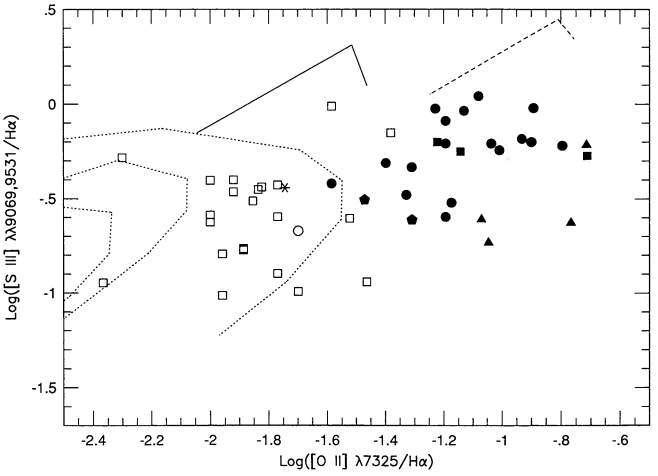

FIG. 5.—Reddening-corrected [S III] λλ9069, 9531/Hα vs. [O II] λ7325/Hα intensity ratios. Symbols and curves as in Fig. 4. Here, asterisk denotes NGC 6221.

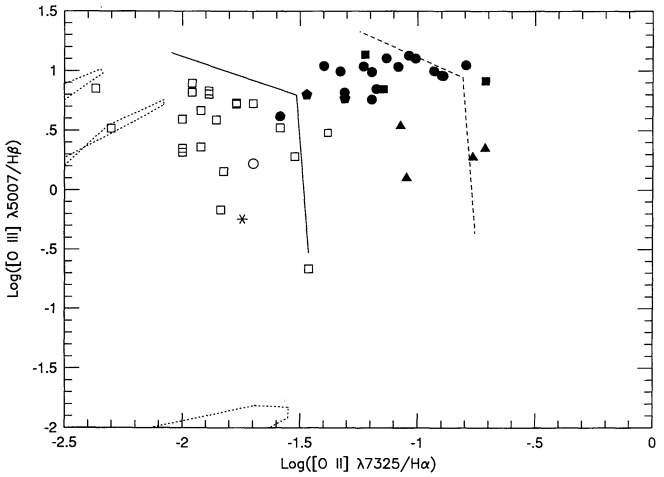

FIG. 6.—Reddening-corrected [O III] λ5007/Hβ vs. [O II] λ7325/Hα intensity ratios. Symbols and curves as in Fig. 4. Here, T_* ranges from 32,500, 40,000, to 55,000 K from bottom to top for the dotted curves, and $\Gamma = 10^{-4}$ at lower right and $\Gamma = 10^{-2}$ at upper left. Asterisk denotes NGC 6221.

Véron, & Zuiderwijk (1981) show that the [O III] lines are much broader (FWHM ~ 520 km s^{-1}) than Hβ (FWHM ~ 100 km s^{-1}), suggesting that the observed spectrum is a superposition of a low-ionization H II region and a high-ionization NLR characteristic of a Seyfert 2 galaxy. Pence & Blackman (1984) confirmed this result, finding from long-slit spectra that the ratio [O III]/Hβ drops from ~2.5 in the nucleus to ~0.2 farther out, again indicating that the nucleus of NGC 6221 probably contains a high-excitation, X-ray ionized source while luminous H II regions exist outside. Combining near-IR data from Morris & Ward (1988) with optical data of Durret & Bergeron (1988), NGC 6221 is characterized by a relatively low [O III]/Hβ ratio and its position on our diagrams tends to be intermediate between the H II–type objects and the Seyfert galaxies. Its line ratios certainly are not consistent either with those of the "pure" Seyferts or the LINERs, a low-ionization emission-line species. Note, however, that they are not greatly different from the ratios found for starburst galaxies, though the number of these in our sample, two, is too small for any conclusive statement.

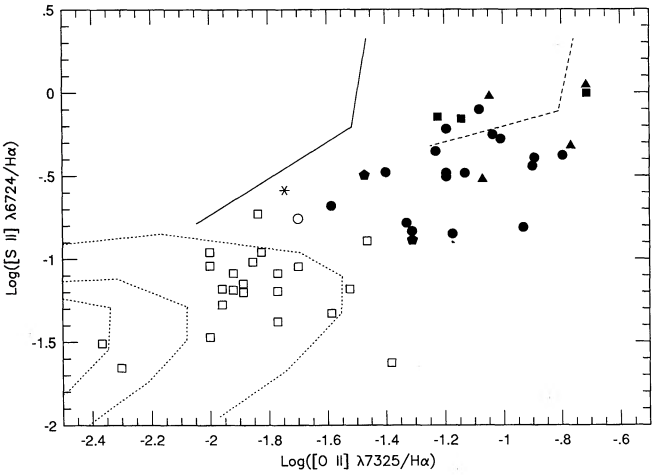

FIG. 7.—Reddening-corrected [S II] λ6724/Hα vs. [O II] λ7325/Hα intensity ratios. Symbols and curves as in Fig. 4. Here, asterisk denotes NGC 6221.

4. DISCUSSION

4.1. *Observed Differences between* H II *Regions and AGNs*

It is clear that the diagrams of Figure 4–7 show quite definite separations between H II region–like objects and the narrow-line regions (NLRs) of AGNs, similar to those seen in VO87. There is essentially no difference in reddening-corrected narrow-line ratios between the Seyfert 1.5 and Seyfert 2 galaxies and they both occupy more or less the same areas. Quantitatively in the near-IR, the mean value of [S III] λλ9069, 9531/Hα for the 12 Seyfert 2 galaxies in our sample is 0.61 ± 0.25, and mean values of [O II] λ7325/Hα is 0.08 ± 0.03. Comparing with the mean values for the 14 Seyfert 1.5 galaxies (including the two "narrow-line Seyfert 1s"), [S III] λλ9069, 9531/Hα = 0.54 ± 0.19 and [O II] λ7325/Hα = 0.08 ± 0.05. This result is in general agreement with Cohen (1983) who found that the average optical narrow-line intensity ratios are very similar in the intermediate Seyfert and Seyfert 2 galaxies. This further suggests that the deblending and separation of the broad and narrow components of the H I Balmer lines have been done approximately correctly. Comparing the [S III]/Hα versus [S II]/Hα diagram with the same one in KP89 shows that the Seyfert galaxy line ratios presented in this study lie in the same region occupied by the six Seyferts in KP89.

We note that there is considerable overlap between the Seyferts and the H II region objects in the [S III]/Hα ratio. This implies that [S III], while analogous to [O III] in many ways, is not as good an indicator of ionization level as [O III], no doubt due to the fact that S^+ has a considerably lower ionization potential (23.3 eV) than O^+ (35.1 eV). However, as Baldwin et al. (1981) stressed, no single ratio can be used to separate AGNs and H II regions unambiguously. Plots of pairs of ratios are far better for such purpose. The diagram which shows the best indication of the continuity between the H II regions, starburst galaxies, LINERs and Seyfert nuclei is Figure 7, in which [S II]/Hα is plotted versus [O II]/Hα. It can be seen that there is a smooth and approximately linear relation between the logarithms of these two quantities, with the Seyfert galaxies and LINERs tending to have larger [S II]/Hα and [O II]/Hα emission line ratios. Thus this diagram is potentially a good tool for separating H II region–type objects from AGNs regardless of their levels of ionization.

Among the diagnostic diagrams based on the near-infrared lines, those which show the clearest separation between the H II regions and the Seyfert galaxies are the plots of [S II]/Hα versus [O II]/Hα (Fig. 7), [S III] λλ9069, 9531/Hα versus [O II] λ7325/Hα (Fig. 5), and [O III] λ5007/Hβ versus [O II] λ7325/Hα (Fig. 6). Several other combinations were tested and proved not as useful. The [O III]/Hβ versus [O II]/Hα diagram is exactly analogous to that of [O III]/Hβ versus [S II]/Hα in VO87. Both give excellent separation between the two classes of objects. As VO87 emphasized, the primary reason for the enhancement of [S II] in AGNs is that they have extended partly ionized zones which do not exist in H II regions. In these large partly ionized zones, ions of H^0, H^+, O^0, and S^+ coexist, allowing collisional excitation to play a dominant role in the emission mechanism of these species. As a result, strong [O I] and [S II] emission lines are produced.

4.2. *Single-Density Photoionization Models*

To guide our interpretation and test our understanding of these diagrams, various models have been plotted for compari-

son with the observed data points. The models are grouped into two major categories: those using one or more hot stars as the source of ionizing radiation characteristic of H II regions, and those assuming a hard power-law continuum as the ionizing source widely thought to be present in AGNs. One set of models assuming photoionization by hot stars was developed for H II regions by McCall, Rybski, & Shields (1985). These models assume a spherically symmetric nebula of uniform density, $N_e = 140$ cm^{-3}, ionized by radiation from stars with effective temperatures ranging from 38,500 to 47,000 K, with heavy-element abundances determined by the ratio O/H, which varies from 0.10 to 4.0 times solar. This sequence is plotted as the dash-dot curve in the diagrams. The paper does not include predictions for the [O II] λ7325 relative intensities.

More recently, Stasinska (1990) calculated a grid of models intended mainly for the study of extragalactic H II regions, to which most of the H II regions in our data sample belong. Her models investigate a wide range both in heavy-element abundance ratios, ranging from 0.01 to 2 times solar, and in effective temperature of the ionizing stars ($T_* = 32{,}500$–$55{,}000$ K). Another input parameter is the number of ionizing stars, which varies from 1 through 10^2–10^4. Spherical symmetry with a uniform density of 10 cm^{-3} is assumed for most models. These models also take into account recombination processes in the formation of forbidden lines of C, N, and O ions. These processes, as noted by Stasinska (1990), are negligible when the heavy-metal abundances are small and the electron temperature therefore relatively high, but become increasingly important for higher abundances. For the [O II] λ7325 blend, she found that the recombination contribution is nearly as large as the collisional contribution at about solar O/H and is dominant for higher O/H. In Figures 4–7 we present a representative sample of her models as three dotted curves, each having a different effective temperature, $T_* = 32{,}500$, 40,000, and 55,000 K, respectively. Along each sequence, the abundances of the heavy elements (C through Fe) range from 0.01 to 2 times solar value. For all the models plotted, the number of ionizing stars is 100 and the density is 10 cm^{-3}. It can be seen from the figures that all the H II region models give fairly good fits to the observed line intensities in our sample, with the exception of the [O III]/Hβ versus [O II]/Hα diagram.

Also plotted in the figures are two sets of photoionization models for AGNs by Stasinska (1984a). The solid curve denotes the model with a spectral index $\alpha = -1.5$ and density $N_e = 10^3$ cm^{-3}, while the dashed line represents one with $\alpha = -1.0$ and $N_e = 10^4$ cm^{-3}. Solar abundances were assumed and the ionization parameter Γ varies from 10^{-2} to 10^{-4} in both models. These models are identical to those called sequence "B" and "C" by KP89 for their [S II]/Hα versus [S III]/Hα diagram. In these figures, there seems to be a disagreement between the measured, reddening-corrected [S III]/Hα ratios and the values predicted for AGN model. The observed values are approximately 3 times lower than predicted, confirming the result noted by KP89 in their much smaller Seyfert sample. Taken at face value, the simplest interpretation would be that the relative abundance of S in Seyfert galaxies is on the average approximately 3 times lower than solar, contrary to the statement by KP89, which seems to be in error, that there is an enhancement of S in these galaxies. Similar conclusions regarding the abundance of S and generally of the heavy metals as a group in AGNs have also been made by Ferland & Netzer (1983) and noted by VO87, based on their comparisons between observed optical line intensities of [S II] and [O I] and predictions from one-density models. Note that it would be difficult, purely on the basis of nucleosynthesis, to explain an AGN S/O abundance ratio one-third of solar. It also contradicts the observational determination by Evans & Dopita (1987) that in H II regions in Seyfert galaxies, S/O is essentially the solar ratio, although of course this may not apply to the nucleus. We emphasize that the models used in these and the present study are simple, one-component models which no doubt oversimplify the real situation, and that any abundance conclusions based on them are therefore crude and uncertain.

4.3. *Multidensity Photoionization Models*

More sophisticated and presumably more realistic, multicomponent, power-law photoionization models exist for AGNs (Stasinska 1984b; Binette 1985; Pequignot 1984), and predictions from one set of such models have been used in the analysis of the optical data in VO87. However, no predicted intensities for [S III] $\lambda\lambda$9069, 9531 intensities were given by Stasinska (1984b), and the models of Pequignot (1984) and Binette (1985) are developed more especially for LINERs rather than Seyferts. Thus we have not been able to compare our observational data with multidensity model predictions. It is well known, however, that including additional higher density components in a single low-density component model tends to increase the inferred abundances which best fit the observed AGN spectra. Therefore, the underabundance of S, if it exists, may actually be less than the factor ~ 3 stated above. If this subsolar heavy-element abundance proves to be real, it will provide important clues toward solving the [O III] temperature problem and the origin and evolution of the emitting gas in AGNs (Tadhunter, Robinson, & Morganti 1989).

4.4. *Other Possible Effects*

It is known that models assuming photoionization as the only energy input mechanism cannot fully explain all observed characteristics of these objects, despite their many notable successes in reproducing the general features of the spectra of observed AGNs. As discussed in § 3, some line ratios such as [S III] $\lambda\lambda$9069, 9535/Hα do not fit such model predictions unless a depletion of heavy elements is invoked. Another current problem is the higher temperatures indicated by the [O III] (λ4959 + λ5007)/λ4363 ratio, in the NLR of Seyfert 1, Seyfert 2, and narrow-line radio galaxies (NLRGs), than those expected from the equilibrium between photoionization alone and radiative cooling (Cohen & Osterbrock 1981; Osterbrock 1983). Recently, the [O III] temperature problem has also been discussed with regard to the extended emission line regions (EELRs) of AGNs by Robinson (1989) and Tadhunter et al. (1989). As suggested by these authors, the higher temperature in AGNs may be due to heating, in addition to photoionization, by interactions of the line-emitting gas with fast charged particles, particularly high-energy relativistic electrons, which are known to be responsible for the radio-frequency emission observed in many active galaxies. This extra nonradiative heating source could explain the higher temperature, which may explain the enhancement of line ratios such as [O II] λ7325/Hα as well as [N II] (λ6548 + λ6583)/Hα in the optical region. A similar source of heating was suggested by Bland-Hawthorn, Sokolowski, & Cecil (1991) to explain the exceptionally high [N II]/Hα ratio observed outside the nucleus of NGC 1068.

The influence of a relativistic electron flux on a standard

photoionization model of AGN emission-line regions has been discussed quantitatively by Ferland & Mushotzky (1984) and Cesar, Aldrovandi, & Gruenwald (1985). They found that the effect of "cosmic rays" is mainly in heating the gas, although they can also slightly modify the ionization levels of various ions within it. Because of the higher temperature, many low-ionization lines are strengthened while some, like Fe II lines, which are no longer formed by the dominant stages of ionization, are actually weakened. Gruenwald & Viegas-Aldrovandi (1987) calculated an extensive grid of single-density component models for AGNs, taking into account the presence of relativistic electrons in the line-emitting regions. More recently, Viegas-Aldrovandi & Gruenwald (1988) computed "integrated" models for the NLRs of AGNs which include a distribution of emission cloud densities ranging from 10^2 to 10^6 cm^{-3}. They considered both radiation-bounded and matter-bounded clouds. In comparing their calculated results with observed optical line ratios, their general conclusion was that although the effect of density stratification is important in photoionization models, its inclusion is not sufficient to explain all the observed line ratios. They argued that relativistic electrons are also needed to improve the fit between the observations and theoretical predictions, at least for the high-ionization lines. Concerning the low-ionization lines, however, they concluded that even if both of the above factors were considered, line ratios for a large number of objects in their study still remain unexplained with radiation-bounded models. To fit these objects with calculated models, Viegas-Aldrovandi & Gruenwald (1988) suggest that the line-emitting clouds must be matter-bounded. This amounts to a reduction in size of the emitting volume and of the transition zone.

In order to examine quantitatively the importance of extra heating by relativistic electrons on the near-infrared emission-line spectra of AGNs, we compare model calculations which include this effect with the data sample of our study. Unfortunately, the published "integrated" model calculations of Viegas-Aldrovandi & Gruenwald (1988) do not include the near-IR lines [O II] $\lambda\lambda$7325 and [S III] $\lambda\lambda$9069, 9531. Therefore, we were forced to use simple single-component models tabulated in Gruenwald & Viegas-Aldrovandi (1987). To take into account a range of densities in the NLR, we show in Figures 8–11 the calculated sequences of models along which N_e varies from 10^2 cm^{-3} to 10^6 cm^{-3} for two values of the ionization parameter Γ (10^{-2} and 10^{-3}). Solid curves represent AGN models assuming solar heavy-element abundances, and photoionization by a broken power-law spectrum with $\alpha_X = 1.7$ and $\alpha_{UV} = 2.5$. They include no contribution from relativistic electrons. The dashed curves represent the models with relativistic electrons added in an amount such that the ratio of relativistic electron flux to the total H density in the cloud is 10^5 cm s^{-1}. It can be seen that except for Figure 10 showing [O III]/Hβ, the diagrams involving [S III]/Hα (Figs. 8 and 9), and to a lesser extent [S II]/Hα and [O II]/Hα (Fig. 11), indicate that the theoretical models give quite poor fits to the observed line ratios, often overpredicting them. Note that in the [O III]/Hβ versus [O II]/Hα diagram (Fig. 10), the observed intensity ratios for AGNs can be explained in terms of photoionization alone with a range of densities. Hence, additional heating from relativistic electrons does not seem necessary. Neither, however, does it destroy the agreement. Thus it seems that no combination of densities in the NLR, or the addition of relativistic electrons alone, would improve the fit between observations and model calculations for the S lines.

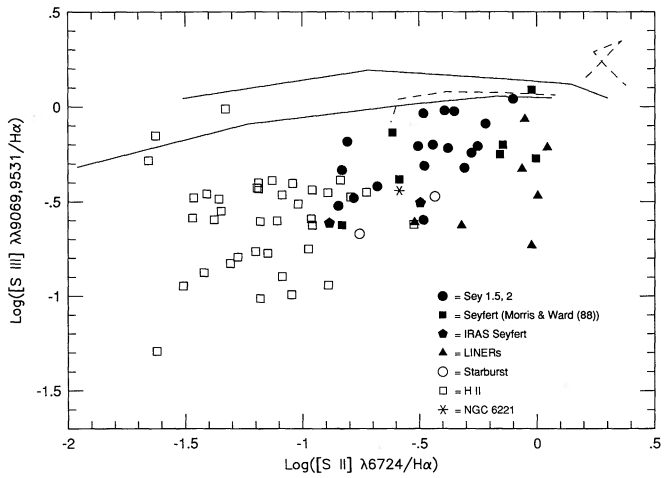

FIG. 8.—Reddening-corrected [S III] $\lambda\lambda$9069, 9531/Hα vs. [S II] λ6724/Hα intensity ratios. The models plotted are from Gruenwald & Viegas-Aldrovandi (1987), showing the effects of density and extra heating from relativistic electrons. The pair of solid curves represents the sequence for $\Gamma = 10^{-3}$ (*upper*) and $\Gamma = 10^{-2}$ (*lower*). Along each curve, N_e varies from 10^2 (*right*) to 10^6 cm^{-3} (*left*). The pair of dashed curves represents the same models after a flux of relativistic electrons has been added.

Similar conclusions were also reached by Viegas-Aldrovandi & Gruenwald (1988) on the basis of the optical lines. They found that the discrepancies can be explained only if the emission line region is matter-bounded *and* some heating by relativistic electrons is included. We cannot confirm this result for the near-IR lines [O II] $\lambda\lambda$7325 and [S III] $\lambda\lambda$9069, 9531 since no matter-bounded theoretical model predictions with the inclusion of relativistic-electron heating have been published for these lines. It seems possible, from the similarity of our results with those in Viegas-Aldrovandi & Gruenwald (1988) for our low-ionization near-IR lines of [S III] and [O II], that matter-bounded emission clouds, coupled with relativistic-electron heating are important in the emission of the low-ionization lines observed in the optical and near-infrared spectral regions of AGNs.

Diaz et al. (1985b) and KP89 have discussed in considerable detail the use of near-infrared line strengths to distinguish

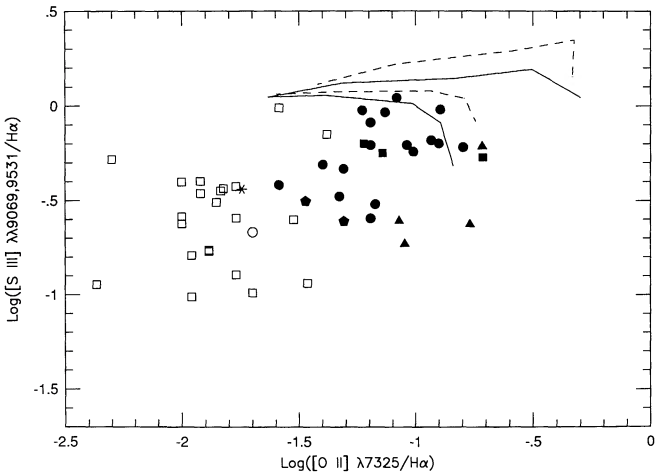

FIG. 9.—Reddening-corrected [S III] $\lambda\lambda$9060, 9531/Hα vs. [O II] λ7325/Hα intensity ratios. Symbols and curves as in Fig. 8, except that $N_e = 10^2$ cm^{-3} at left end of lines and $N_e = 10^6$ cm^{-3} at right.

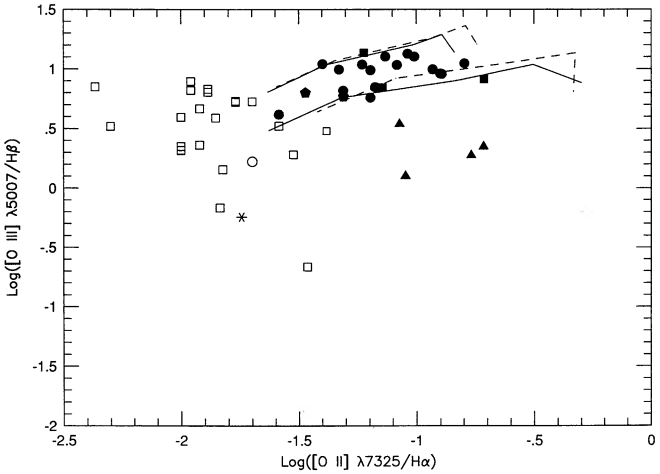

FIG. 10.—Reddening-corrected [O III] λ5007/Hβ vs. [O II] λ7325/Hα intensity ratios. Symbols curves as in Fig. 9. Here, $\Gamma = 10^{-2}$ for the upper curves and $\Gamma = 10^{-3}$ for the lower ones.

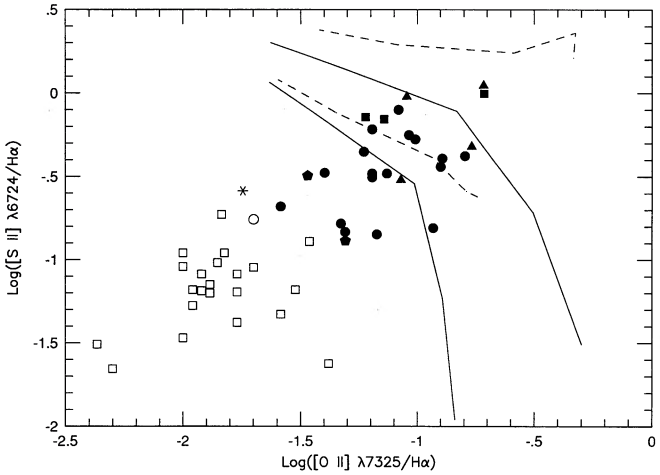

FIG. 11.—Reddening-corrected [S II] λ6724/Hα vs. [O II] λ7325/Hα intensity ratios. Symbols and curves as in Fig. 9.

between shock ionization and other possible ionization mechanisms in AGNs. Diaz et al. argued that the relative strengths of [S II] λ6724 and [S III] $\lambda\lambda$9069, 9531, when used in conjunction with [O II] λ3727 and [O III] $\lambda\lambda$4959, 5007, can be a powerful diagnostic between shocks and photoionization. The observational results of KP89 support this general conclusion but show that these lines *alone* do not unambiguously determine the ionization mechanism. The shock models of Shull & McKee (1979) predict weaker [S III] emission than power-law photoionization models and fall well below the data points of Seyfert 1.5 and 2 galaxies in Figures 4, 5, 8, and 9. This result provides additional evidence that the *dominant* ionization process in Seyfert 1.5 and 2 galaxies is indeed photoionization by a hard spectrum (similar to a power-law continuum). In contrast, LINERs probably constitute an inhomogeneous group of objects in which photoionization by a weak hard spectrum, or a spectrum with a cutoff is the dominant ionization process in some objects while shock ionization dominates in others (VO87; Osterbrock 1991). Both these processes may be taking place in some LINERs. No additional data on LINERs were obtained in the present study, and therefore we can add nothing about the ionization mechanism in these objects.

5. GENERAL CONCLUSIONS

We have obtained deep red and near-IR spectra for a number of Seyfert galaxies in this study. Emission-line intensity measurements from these spectra, together with those of Paper I and other published papers on additional AGNs and H II regions, show that diagrams employing reddening-corrected line ratios of near-IR lines, such as [S II] λ6724/Hα versus [O II] λ7325/Hα, [O III] λ5007/Hβ versus [O II] λ7325/Hα, and [S III] $\lambda\lambda$9069, 9531/Hα versus [O II] λ7325/Hα, provide very good tools for distinguishing AGNs from H II region–like objects. From these and similar diagrams in the optical spectral regions (e.g., VO87), the classification of emission-line galaxies is presently relatively well established and understood. However, the cause of the strong enhancement of lines like [O II] λ7325 and [N II] $\lambda\lambda$6548, 6583 in AGNs over H II regions is still not clear. Higher temperatures in AGNs, perhaps caused by the harder input spectrum or extra heating by relativistic electrons, may provide a natural explanation for the strengthening of these collisionally excited lines. In addition, with our larger sample, we confirm the puzzling discrepancy found by KP89 between the observed intensity ratio of [S III] (λ9069 + λ9531)/Hα and various AGN model predictions in the sense that the models always tend to make this line ratio too large. Subsolar heavy element abundances in AGNs remain a possible but unlikely explanation for this problem. Whether the emission-line regions in AGNs are radiation-bounded or matter-bounded is important and must also be examined fully.

We are very grateful to J. S. Miller, W. G. Mathews, R. W. Pogge, and R. A. Shaw for many illuminating discussions on the subjects of this paper, and to the National Science Foundation for partial support of this research under NSF grant AST 86-11457. H. D. T. would like to thank J. S. Miller for financial support during the later parts of this work under NSF grant AST 88-18925. S. V. would like to acknowledge the financial support of the Natural Sciences and Engineering Research Council of Canada through a postdoctoral fellowship as well as the National Science Foundation through grant AST 88-18900. We are also grateful to the referee, S. L. Morris, for his helpful suggestions on the first version of this paper, which improved it markedly.

REFERENCES

Baldwin, J. A., Phillips, M. M., & Terlevich, R. 1981, PASP, 93, 5
Binette, L. 1985, A&A, 143, 334
Binette, L., Calvet, N., Canto, J., & Raga, A. C. 1990, PASP, 102, 723
Bland-Hawthorn, J., Sokolowski, J., & Cecil, G. 1991, ApJ, 375, 78
Cecil, G., Bland, J., & Tully, R. B. 1990, ApJ, 355, 70
Cesar, M. L., Aldrovandi, M. V., & Gruenwald, R. B. 1985, PASP, 97, 850
Cohen, R. D. 1983, ApJ, 273, 489
Cohen, R. D., & Osterbrock, D. E. 1981, ApJ, 243, 81
Dahari, O. 1985, AJ, 90, 1772
Dennefeld, M., & Stasinska, G. 1983, A&A, 118, 234
De Robertis, M. M., & Osterbrock, D. E. 1986, ApJ, 301, 98
Diaz, A. I., Pagel, B. E. J., & Terlevich, E. 1985a, MNRAS, 214, 41P
Diaz, A. I., Pagel, B. E. J., & Wilson, I. R. G. 1985b, MNRAS, 212, 737
Durret, F., & Bergeron, J. 1988, A&AS, 75, 275
Evans, I. N., & Dopita, M. A. 1987, ApJ, 319, 662
Ferland, G. J., & Mushotzky, R. F. 1984, ApJ, 286, 42
Ferland, G. J., & Netzer, H. 1983, ApJ, 264, 105
Filippenko, A. V. 1985, ApJ, 289, 475

Fosbury, R. A. E., Mebold, U., Goss, W. M., & Dopita, M. A. 1978, MNRAS, 183, 549
Fosbury, R. A. E., & Wall, J. V. 1979, MNRAS, 189, 79
Fried, J. W., & Ulrich, H. 1985, A&A, 152, L14
Garnett, D. R. 1989, ApJ, 345, 282
Gaskell, C. M. 1984, ApJ, 24, L43
Gaskell, C. M., & Ferland, G. J. 1984, PASP, 96, 393
Gruenwald, R. B., & Viegas-Aldrovandi, S. M. 1987, A&AS, 70, 143
Halpern, J. P., & Steiner, J. E. 1983, ApJ, 269, L637
Hummer, D. G., & Storey, P. J. 1987, MNRAS, 224, 801
Kirhakos, S., & Phillips, M. M. 1989, PASP, 101, 949 (KP89)
Koski, A. T. 1978, ApJ, 223, 56
Malkan, M. A. 1983, ApJ, 264, L1
Marshall, F. E., et al. 1979, ApJS, 40, 657
McCall, M. L., Rybski, P. M., & Shields, G. A. 1985, ApJS, 57, 1
Morris, S. L., & Ward, M. J. 1988, MNRAS, 230, 639
Osterbrock, D. E. 1983, in IAU Symp. 103, Planetary Nebulae, ed. D. R. Flower (Dordrecht: Reidel), 473
———. 1985, PASP, 97, 25
———. 1989, Astrophysics of Gaseous Nebulae & Active Galactic Nuclei (Mill Valley: University Science Books)
———. 1991, Rep. Progr. Phys., 54, 579
Osterbrock, D. E., & Koski, A. T. 1976, MNRAS, 176, 61P
Osterbrock, D. E., & Pogge, R. W. 1985, ApJ, 297, 166
Osterbrock, D. E., & Shaw, R. A. 1988, ApJ, 327, 89
Osterbrock, D. E., Shaw, R. A., & Veilleux, S. 1990, ApJ, 352, 561 (Paper I)
Osterbrock, D. E., Tran, H. D., & Veilleux, S. 1992, ApJ, in press
Pence, W. D., & Blackman, C. P. 1984, MNRAS, 207, 9
Pequignot, D. 1984, A&A, 131, 159
Perez, E., Manchado, A., Garcia-Lario, P., & Pottasch, S. R. 1990, A&A, 227, 407
Phillips, M. M. 1979, 227, L121
Phillips, M. M., Charles, P. A., & Baldwin, J. A. 1983, ApJ, 266, 485
Phillips, M. M., Jenkins, C. R., Dopita, M. A., Sadler, E. M., & Binette, L. 1986, AJ, 91, 1062
Phillips, M. M., Pagel, B. E. J., Edmunds, M. G., & Diaz, A. I. 1984, MNRAS, 210, 701
Robinson, A. 1989, in ESO Workshop on Extranuclear Activity in Galaxies, ed. E. J. A. Meurs & A. E. Fosbury (Garching: ESO), 259
Shields, G. A., & Oke, J. B. 1975, PASP, 87, 879
Shuder, J. M. 1980, ApJ, 240, 32
Shull, J. M., & McKee, C. J. 1979, ApJ, 227, 131
Stasinska, G. 1984a, A&AS, 55, 15
———. 1984b, A&A, 135, 341
———. 1990, A&AS, 83, 501
Tadhunter, C. N., Robinson, A., & Morganti, R. 1989, in ESO Workshop on Extranuclear Activity in Galaxies, ed. E. J. A. Meurs & A. E. Fosbury (Garching: ESO), 293
Veilleux, S. 1991, ApJ, 368, 158
Veilleux, S., & Osterbrock, D. E. 1987, ApJS, 63, 295 (VO87)
Véron, M. P., Véron, P., & Zuiderwijk, E. J. 1981, A&A, 98, 34
Viegas-Aldrovandi, S. M., & Gruenwald, R. B. 1988, ApJ, 324, 683
Wampler, E. J. 1971, ApJ, 164, 1